Journal of Food Composition and Analysis 151 (2026) 108951

Contents lists available at ScienceDirect

Journal of Food Composition and Analysis

journal homepage: www.elsevier.com/locate/jfca

Detection of kiwifruit low-force early bruise by combining surface textural parameters and near-infrared hyperspectral imaging

Irene Locatelli [a], Silvia Grassi [a,*], Alessandro Grassi [a], Giulia Gorla [b], José Manuel Amigo [b,c]

[a] Department of Food, Environmental and Nutritional Sciences, University of Milan, Via Celoria 2, Milano 20133, Italy
[b] Department of Analytical Chemistry, Faculty of Science and Technology, University of the Basque Country UPV/EHU, Sarriena s/n, Leioa, Basque Country 48940, Spain
[c] Ikerbasque, Basque Foundation for Sciences, María Díaz de Haro, 3, Bilbao 48013, Spain

ARTICLE INFO

Keywords:
Actinidia deliciosa
Kiwifruit
Damage detection
NIR-HSI
Surface Texture Analysis

ABSTRACT

This study evaluates the feasibility of detecting and monitoring occurrence and progression of low-force mechanical damage in kiwifruit (*Actinidia deliciosa*) using Near-Infrared Hyperspectral Imaging combined with surface texture analysis and multivariate classification. Previous studies have applied HSI for bruise detection but often used unrealistically high impact forces, limiting relevance to real-world handling conditions. 'Hayward' kiwifruit were subjected to controlled impact forces of very low intensity (23.4 N and 46.8 N) to simulate realistic damage and stored at 25 ± 1 °C for five days. Hyperspectral data were acquired using a short-wave infrared camera (960–2500 nm) at different sampling times. Principal Component Analysis (PCA) was applied to reduce data dimensionality, and surface texture features extracted from PCA score images accounted for fruit shape and surface characteristics. A Partial Least Squares – Discriminant Analysis (PLS-DA) model classified damaged versus healthy tissue, achieving an overall accuracy of 94.7 % across hyperspectral images. Changes in damaged pixels allowed an indirect evaluation of progressive tissue degradation.

Results showed a high detection of damaged (invisible to naked eye) and healthy tissue, demonstrating the efficiency of the methodology in preventing fruits affected by realistic damage from entering the fresh market while facilitating their use in alternative applications.

1. Introduction

The kiwifruit (*Actinidia deliciosa*) is gaining economic importance due to its rich nutritional profile, which includes vitamins, minerals, and dietary fibre (Ebrahimi et al., 2023). Its sensory characteristics also contribute to its global appreciation. However, the soft texture and high-water content of kiwifruit make them particularly susceptible to mechanical damage. This vulnerability critically emerges at all stages of the production chain, from harvesting to logistics (Hou et al., 2023). Mechanical damage not only harms the appearance of the fruit but also shortens its shelf life, negatively impacting marketing and consumer acceptance, with financial implications for producers and the entire supply chain (Barrett et al., 2010). Therefore, it is crucial to implement effective damage detection methods during pre-harvest and post-harvest stages to prevent economic losses and ensure customer satisfaction.

Mechanical damage, such as bruising, compression, or tearing, may not be immediately visible after the initial impact and can worsen over time. This makes early detection and maintaining high standards more difficult. Unlike other varieties, such as apples and pears, damage in kiwifruit may remain hidden under the skin (Ahmadi, 2012), making its detection particularly challenging. Conventional techniques for assessing fruit quality, which rely on visual inspection or destructive analysis of physicochemical parameters, have considerable limitations. For example, visual inspections may overlook internal damage that is not immediately apparent, whereas destructive measurements irreversibly alter the fruit, making them unsuitable for large-scale quality control applications (Mahanti et al., 2022). Furthermore, these approaches require specialized personnel and are time-consuming, not allowing the inspection of each fruit on fast-moving processing lines.

In commercial practice, bruise detection is commonly implemented using LED illumination, typically around 900 nm, combined with computer vision and artificial intelligence (AI) for pattern recognition. These systems enable the rapid, automated sorting of fruit on industrial lines and have also been applied to kiwifruit. However, the accuracy of such

* Corresponding author.
E-mail address: silvia.grassi@unimi.it (S. Grassi).

https://doi.org/10.1016/j.jfca.2026.108951
Received 18 August 2025; Received in revised form 22 January 2026; Accepted 26 January 2026
Available online 27 January 2026

commercial approaches remains limited, particularly for detecting early or subtle internal damage (Bu et al. 2024a,2024b; Lü et al., 2011). This limitation motivates the exploration of hyperspectral imaging (HSI) techniques, which capture a broader spectral range and provide detailed chemical and structural information, potentially enhancing sensitivity and specificity in damage detection. To address these challenges, there is a growing interest in the development of non-destructive techniques that allow early detection of mechanical damage without compromising product integrity. Near-Infrared Hyperspectral Imaging (NIR-HSI) could be a valid alternative, offering rapid and non-invasive damage assessments at both surface and internal levels. Indeed, by a wide wavelength range of the electromagnetic spectrum, HSI is able to capture, to a certain degree, detailed information on the internal composition and physical properties of the fruit (Amigo, 2019), revealing chemical and structural changes not visible to the human eye (Tanzilli et al., 2024). In this context, NIR-HSI emerges as a promising solution. Short-wave NIR wavelengths are sensitive to variations in water distribution and tissue microstructure, which makes this technique suitable for detecting even low-impact mechanical damage before bruises become externally visible (Liang et al., 2025).

Previous studies have shown that HSI can successfully detect mechanical damage in kiwifruit (Gao et al., 2021; Bu et al. 2024a,2024b; Liu et al., 2019). However, a crucial aspect of the current research is the impact force applied during testing. Whereas previous studies have used forces between 100 and 200 N to simulate mechanical damage (Gao et al., 2021; Bu et al. 2024a,2024b), applying significantly lower forces, even one-third of those used previously, should be considered to address more realistic impact conditions. Indeed, mechanical damage in kiwifruit is often caused by not severe impacts, such as those occurring during daily harvesting and transport. In the study conducted by Adewoyin (2023), the force levels considered reflect the actual conditions that kiwifruit may encounter, emphasising the need for realistic simulations. Specifically, Ahmadi (2012) estimate different levels of damage (force, N) according to the supply chain step considered, mainly a high damage (76.16 N) occurring during mechanical harvesting, a moderate damage (41.57 N) during handling, and a low damage (23.73 N) during transport. Thus, although various studies in the literature demonstrate a correlation between NIR-HSI and kiwifruit bruising, none of them have investigated the occurrence of damage induced by a realistic force.

Within this framework, the present work aims to demonstrate the reliability of NIR-HSI technology for monitoring mechanical damage in kiwifruit under realistic low-force damage conditions. Accurate, non-destructive damage detection will enable producers to make more informed decisions regarding fruit distribution and to avoid the marketing of damaged produce. This not only protects the economic value of the product but also helps to meet growing consumer expectations regarding food quality and freshness.

2. Material and methods

2.1. Kiwifruit sampling

Five batches of kiwifruit (*Actinidia deliciosa*, variety *Hayward*) were purchased from local grocery stores in Bilbao (Spain) on five different weeks in April 2024 (batch 1), May 2024 (batch 2), November 2025 (batches 3 and 4) and December 2025 (batch 5). Fruits were selected based on uniform size (7.0 cm length, 4.8 cm diameter) and with soluble solid content close to the commercial ripening stage (12.7 ± 0.97 °Brix) (Koutsoflini et al., 2013) to minimize variability in mechanical properties. Throughout the study, the fruits were damaged according to the procedure described in section §2.2 and stored at room temperature (T = 25 ± 1 °C) up to 5 days after purchasing. The fruits were handled with care during the experiments to avoid unintentional bruising or secondary damage and reduce the probability of unintended damage.

2.2. Damage induction and experimental procedure

Mechanical damage was induced using a controlled configuration. A weight was dropped from a height of 1 m through a vertical tube, ensuring a precise and constant impact on the fruit at the base. The cylindrical weight of 34.61 g had a diameter of 14.5 mm, a height of 50.5 mm and was composed of metal to ensure uniform mechanical properties.

Three distinct experimental conditions were applied (Table 1): a) Control (CC): Fruit without mechanical damage; b) Standard weight (SW): A weight of 34.61 g applied with the flat base of the cylinder in contact with the fruit; c) Double weight (DW): A weight of 69.22 g applied with the flat base of the cylinder in contact with the fruit. The potential energy for SW was calculated at approximately 0.3396 Joules, the impact force estimated to be approximately 23.4 N, the double for DW experimental conditions (approximately 46.8 N), i.e., mimicking low damage occurring during transport and moderate damage occurring during handling, respectively (Ahmadi, 2012).

After the impact, the analyses were carried out for five consecutive days for the kiwifruit of batch 1 and 2, during which hyperspectral images of each of the 12 kiwifruit were acquired daily to monitor the occurrence and progression of damage, for a total of 67 images (Table 1). For batches 3–5, CC kiwifruit were analysed the day of purchasing, whereas the images of DW were acquired after 5 days of storage at 25 ± 1 °C, for a total of 16 images (Table 1). Digital images of whole and peeled kiwifruit were collected after NIR-HSI analysis to assess the damage location and possible secondary damage.

2.3. NIR hyperspectral imaging (HSI) system

Hyperspectral images were acquired with a SWIR Hyperspectral camera (Specim Spectral Imaging Ltd, FIN-90571 Oulu, Finland), which covers the NIR range from 996 nm to 2505 nm. The camera operates with a spatial resolution of 320 pixels per line scan and a spectral resolution of 5 nm, allowing fine variations in the spectral properties of kiwifruit to be detected. The system was configured for each acquisition with an exposure time of 5 ms, ensuring an adequate signal-to-noise ratio without overexposing the images. The frame rate was set at 100 Hz, allowing for rapid acquisition of spectral data, while the scan rate was kept at 22 mm/s to ensure steady and smooth movement of the samples during image acquisition. These parameters were chosen to optimize the balance between image clarity and acquisition efficiency, reducing the risk of motion artifacts that could affect the accuracy of damage detection. The samples were illuminated using halogen lamps placed at 45 ° with respect to the detector.

Table 1
Sample identification.

Week	Control (CC)	Standard weight (SW)	Double weight (DW)
Batch 1 (2024)	K01_CC (from T0 to T5)	K05_SW (from T0 to T5)	K09_DW (from T0 to T4)
	K02_CC (from T0 to T5)	K06_SW (from T0 to T4)	K10_DW (from T0 to T5)
Batch 2 (2024)	K03_CC (from T0 to T4)	K07_SW (from T0 to T5)	K11_DW (from T0 to T5)
	K04_CC (from T0 to T4)	K08_SW (from T0 to T4)	K12_DW (from T0 to T5)
Batch 3 (2025)	K13_CC (T0)		K21_DW (T5)
	K14_CC (T0)		K22_DW (T5)
	K15_CC (T0)		K23_DW (T5)
Batch 4 (2025)	K16_CC (T0)		K24_DW (T5)
	K17_CC (T0)		K25_DW (T5)
	K18_CC (T0)		K26_DW (T5)
Batch 5 (2025)	K19_CC (T0)		K27_DW (T5)
	K20_CC (T0)		K28_DW (T5)

K, kiwifruit number identification, CC, control, SW, single weight, DW, double weight, T0-T5, day of storage

During the five consecutive days of image acquisition, special care was taken to maintain the constant orientation and positioning of the fruit. The fruits were manually repositioned each day to match the initial orientation, and the acquisition window was kept constant at all time points to ensure spatial consistency of the hyperspectral data.

The camera was calibrated using the spectra obtained from a Spectralon plate (white reference) and the spectra obtained from the camera with the lenses covered by the shutter (dark reference). The diffuse reflectance was transformed into log10(1/R) units following standard procedures (Ozaki et al., 2020).

2.4. Data analysis

Data exploration and analysis were conducted in the MATLAB environment (v. R2021b, MathWorks, Inc., Natick, MA, USA) using the HYPER-Tools Toolbox (v. 3.0) (Mobaraki, Amigo 2018) (freely available at https://www.hypertools.org/, last accessed July 2025).

The background was removed using a threshold (< -0.001) to the 21st spectral band of the first derivative (Savitsky Golay, 15 window points, third polynomial order) of the pre-processed image. This threshold was determined empirically to exclude only non-informative background regions and applied consistently to all hyperspectral images in the dataset. Masked pixels were excluded from further analysis to improve data quality and prevent noise interference from influencing subsequent analyses (Arbash et al., 2023).

Each hyperspectral image had an original size of 320 × 3000 pixels. To ensure consistency across the dataset and improve computational efficiency, each image was first resized to 100 × 100 pixels using bicubic interpolation. After resizing, the images were assembled into a single augmented hyperspectral image for the 2024 dataset, i.e. batch 1 and 2, by arranging them in a grid format, resulting in a final size of 1200 × 600 pixels. Similarly, an augmented image was created for 2025 dataset (400 × 400).

Principal component analysis (PCA) was then applied as an unsupervised exploratory technique to analyse the spectral data and identify patterns of variance between samples. PCA was performed on the standard normal variate (SNV)-corrected hyperspectral data, and the principal components were analysed to assess their contribution to the variance of the dataset (Mobaraki, Amigo, 2018). Surface textural features were calculated following the methodology proposed by Bharati et al. (2004). To consider the spatial structure of the bruises, 2 PCs of the PCA model were selected, and each of these PCs was then processed using a sliding window approach with a window size of *n* pixels applied in four directions (up, down, left, and right). This approach enables the extraction of spatial correlation patterns by evaluating the local variations of each PC, effectively enhancing the identification of structured information within the hyperspectral image. In this case, *n* accounted for 2 and 3 pixels, considering the relative size of the bruise in comparison with the relative size of the kiwifruit. Therefore, an image containing surface texture parameters (1200 × 600 × 18) was obtained, where the 18 variables consisted of the 2 selected PCs and the corresponding slicing images in the 4 directions (0, 90, 180 and 270°) for each PC.

The data collected in 2025 were projected in the built PCA space, and the same approach was used to extract surface texture information, obtaining an image of 400 × 400 × 18.

A PLS-DA model was trained by manually selecting (1) candidate pixels from one clearly damaged fruit area as the damaged class, and (2) candidate pixels from one control fruit as the healthy class. The classification performance was assessed by 10-fold Venetian blinds cross-validation. The predictive accuracy of PLS-DA was evaluated both on the entire 2024 dataset (67 images) and the 2025 dataset (16 images).

To visualise the classification results, a false-colour image was created, in which each pixel was assigned to either the damaged or healthy class. To reduce the influence of isolated pixels likely caused by noise or imaging artifacts, a region was considered as 'damage area' only when at least 20 contiguous pixels were classified as damaged. The percentage of damage region was then calculated as the ratio of damaged pixels to the total number of pixels belonging to a specific fruit.

3. Results and discussion

3.1. Preprocessing of hyperspectral data and spectral features

After background removal, the spectral characteristics of control kiwifruit samples were investigated to identify key absorption bands in the NIR region. Fig. 1(a) shows the fake-RGB images of three CC kiwifruit samples at time zero (K03_CC, K08_CC and K11_CC), where three specific points were selected on each fruit, one in the medium-upper region (orange), one near the central area (green), and one on the lateral surface (blue). The three points were selected to highlight differences possibly related to the fruit geometrical shape within the produce variability. The corresponding spectra in Fig. 1(b) exhibit a similar spectral shape but with vertical shifts, indicating that while the overall chemical composition remains consistent, differences in light penetration and geometry may affect reflectance intensity. Indeed, spectra selected in the central area (green), i.e. the ones closest to the NIR-HSI camera and less affected by the round shape, are the ones with highest reflectance, whereas the spectra selected in the lateral surface (blue) close to the fruit boundary were characterised by the lowest reflectance possibly due to highest distance from the camera and edge artefacts. The medium-upper spectra (orange) were characterised by intermediate reflectance. Such spatial differences are consistent with the strong dependence of light propagation on the local optical properties of fruit tissues reported for kiwifruit pulp and peel (Cheng et al., 2022).

However, since the hyperspectral images were acquired using a fixed setup and each fruit was manually repositioned to maintain a consistent orientation throughout the five days of acquisition, the influence of geometric variability was minimized. This strengthens the interpretation that observed spectral differences reflect internal variations rather than artefacts due to acquisition geometry.

The analysis of the raw spectra revealed four major absorption peaks associated with O–H and C–H molecular vibrations, typically linked to water, carbohydrates, and cell wall components (Ciccoritti et al., 2019). The 1074 nm peak corresponds to C–H second overtone stretching, indicative of sugars and carbohydrates (Magwaza et al., 2012), whereas the 1270 nm band is related to O–H stretching overtones, characteristic of water absorption and hydrogen bonding in biological tissues (Fu et al., 2007). The 1660 nm absorption arises from a combination of O–H and C–H stretching vibrations, often associated with pectin and water interactions in fruit tissue (Ma et al., 2021). Lastly, the 1883 nm peak corresponds to O–H bending modes, reinforcing the strong presence of water absorption bands. Although these peaks align with general NIR absorption patterns in fresh produce, some differences emerge when compared to previous studies. For instance, Ma et al. (2021) reported absorption bands at 1200 nm, 1450 nm, and 1930 nm, commonly linked to water and carbohydrate interactions. These shifts in peak positions may be attributed to differences in fruit variety, moisture content, or optical path length in the hyperspectral imaging setup (Magwaza et al., 2012).

To evaluate the effect of damage over time, the raw and pre-processed spectra of a specific point referred to a damaged fruit (*K05_SW* from T0 to T5) were visually evaluated. One specific pixel, presumably damaged by the weight impact, was selected for each sampling time (Fig. 2a). The selected pixels were plotted as raw (Fig. 2b) and after transformation by SNV (Fig. 2c). The raw spectra reflectance appeared like those selected for control kiwifruit evaluation (Fig. 1b), even if the band at 1074 nm, i.e., the C–H second overtone stretching indicative of sugars and carbohydrates, seemed sharper than the one observed for control fruits. Furthermore, the decrease in reflectance of the band at 1660 nm, often associated with pectin and water interactions in fruit tissue (Ma et al., 2021), resulted in a more intense signal than for control kiwifruit. However, due to baseline changes,

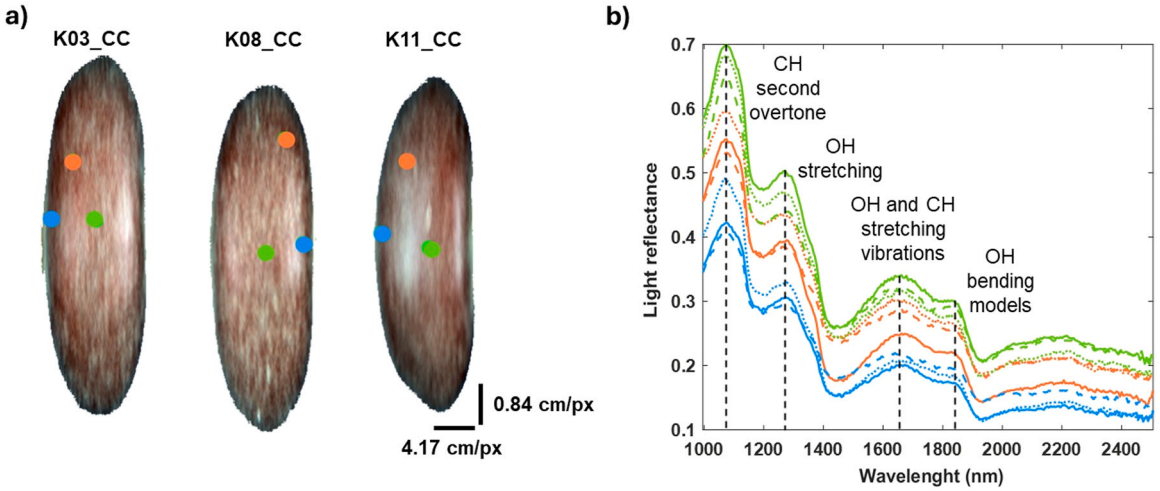

Fig. 1. Fake-RGB image of three kiwifruit samples at time zero, with selected points for spectral extraction (blue: edge, orange: intermediate, green: centre) (a), corresponding raw spectra (b) (Line = K03_CC_T0; Dots = K08_SW_T0; Dashed line = K11_DW_T0).

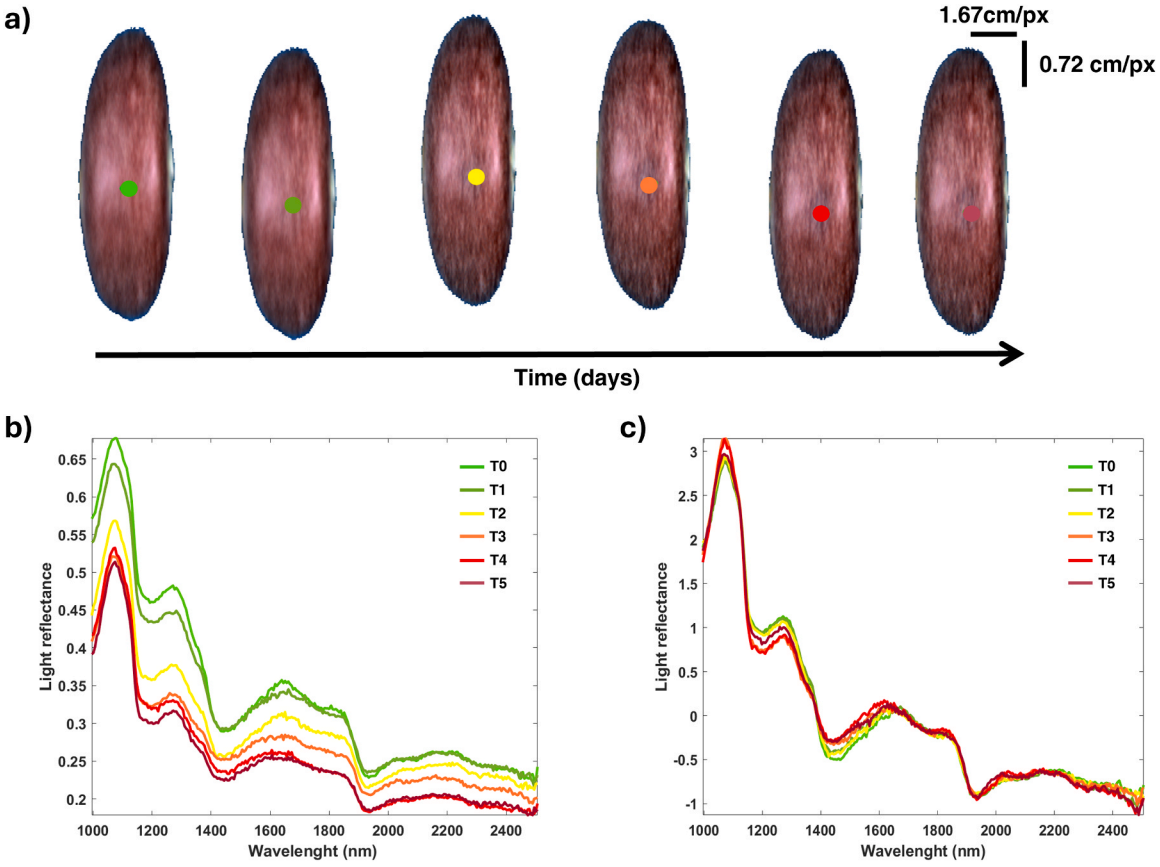

Fig. 2. Fake-RGB image of one kiwifruit samples at different time points (K05_SW from T0 to T5) with selected points to highlight spectral changes in selected damaged areas (a), selected raw spectra (b), selected pre-processed spectra after SNV (c).

direct interpretation can be difficult.

Notably, a general reduction in raw reflectance was observed over time, particularly in the spectral window from approximately 1200–1900 nm. This trend can be explained by the progressive redistribution of water within the fruit tissue following mechanical damage. Liang et al. (2025) demonstrated that bruised kiwifruit undergoes a dynamic shift in water states from vacuolar to intercellular and cytoplasmic compartments, together with moisture loss through evaporation and respiration. These processes, together with microstructural degradation, alter light scattering and absorption behaviour, resulting in reduced reflectance values over time in the damaged areas.

SNV transformation corrected baseline variations and minimized scattering effects, enhancing the comparability of spectra across different sampling times (Fig. 2c). The transformed spectra enhanced the differences at 1270, 1450, and 1660 nm in the spectra collected from the damaged area over time, suggesting the possibility of detecting changes in water distribution, cell wall breakdown, and other biochemical changes that occur in damaged regions over time. Similar

behaviour was observed for neighbouring pixels, presumable referring to damaged areas.

3.2. PCA and surface texture image

The results of the PCA on the augmented image of 2024 dataset are displayed in Fig. 3. In the PC1 score image, the central areas of the fruits are characterised by high positive PC1 values due to the positive load of the region from 1500 nm to 1900 nm. As observed in the raw spectra (Fig. 1a), the central convex area is characterised by higher reflectance in this spatial region than in the fruit edges, as strongly influenced by the round shape of the samples, suggesting that the main variations captured are related to scattering effects and geometric differences rather than substantial chemical changes. Even if Gaston, Frias, Cullen, O'Donnell, & Gowen (2010) reported that scatter correction strategies could correct curvature effects in large objects, such as mushrooms, in our case, the curvature of the fruit seems to be the dominant effect being the main feature described by PC1 (56 % of the explained variance) as observed for smaller products, such as kernels (Manley et al., 2012; Delwiche et al., 2021).

Presumably, damaged areas exhibited negative PC2 and PC4 scores in the PC score surface image, which was highly influenced by the band in the region between 1200 and 1300 nm, where changes are sensitive to water content and bond, and cellular matrix degradation (Gowen et al., 2007). The association between PC2 and PC4 and damage is, therefore, plausible, suggesting that these components may be an effective indicator to identify structural and physiological changes in the fruit.

Once this analysis was done, the PCs were submitted to the sliding procedure to highlight the fact that the damage can be somehow visible on the score surfaces. Still, their presence is because those damaged areas have a different spatial configuration than other areas of the kiwifruit.

3.3. PLS-DA

To develop the PLS-DA classification model, spectra from two fruits were selected for calibration and cross-validation, whereas the entire dataset (2024 or 2025) was used for external prediction. Specifically, during the calibration phase, a set of 100 spectra from K2_CC_T5 was selected as non-damage kiwifruit, whereas a set of 100 spectra from K5_SW_T5 was used to represent the damaged class.

The calibration model showed good performance: reaching an accuracy of 99 %, a sensitivity of 97 % and a specificity 99 % for the

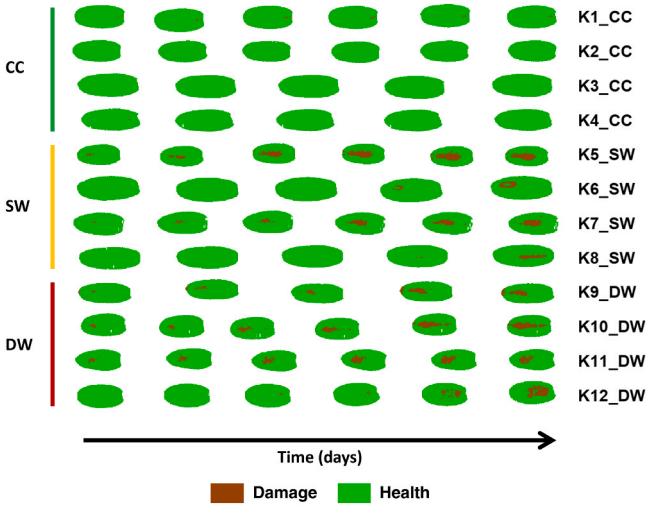

Fig. 4. False-colour RGB images representing PLS-DA predictions of damaged and healthy tissue in batches 1–2 of kiwifruits. Damaged areas are highlighted (red), showing the progression of mechanical damage over time.

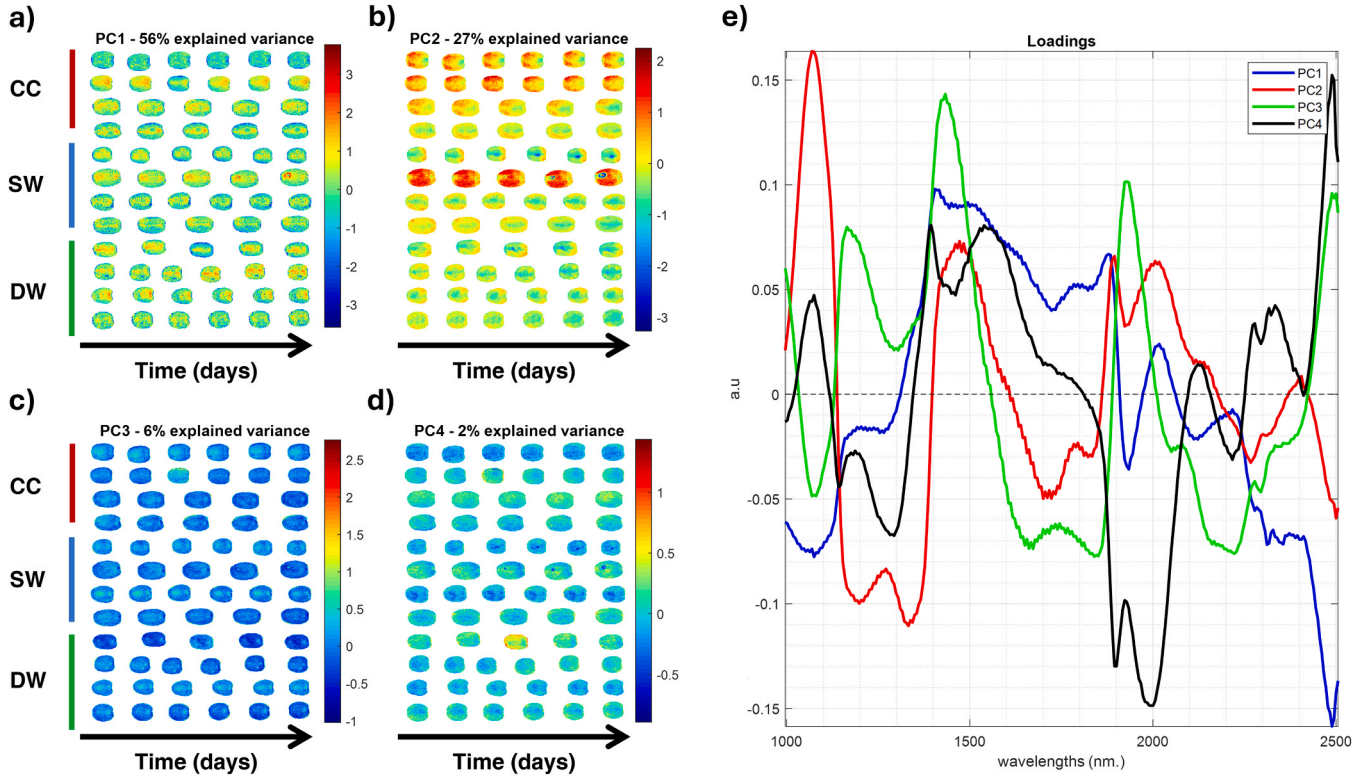

Fig. 3. PCA results from SNV-preprocessed hyperspectral images of batches 1–2: score surfaces of PC1(a), PC2 (b), PC3 (c), PC4 (d), and the corresponding loading plot (e).

damage class both in calibration and cross-validation. Prediction results on the 2024 dataset are shown in Fig. 4 as a false colour RGB-images.

To evaluate whether the pixels classified as damage correspond to real tissue damage area, considering both induced mechanical damage and secondary damage, false colour RGB-images from batch 3, 4 and 5 (2025 dataset) were compared with RGB images of whole and peeled fruits (Fig. 5). Overall, this comparison showed that most CC fruits showed no visible damage in the RGB images, as predicted by the PLS-DA model. However, some pixels in K13_CC and K15_CC were classified as damaged. In K13_CC, pixels predicted as damaged (17.33 % of the total kiwifruit) corresponded to lesions visible in the peeled fruit, likely representing secondary damage. For K15_CC, pixels classified as damaged (10.26 % of the total kiwifruit) appear to be false positives, likely due to light interference. In any case, there is good correspondence between predicted damaged pixels and the bruises visible in the peeled fruits subjected to induced mechanical damage (Fig. 5).

These results align with previous studies showing that early bruising in kiwifruit can induce subtle but measurable alterations in optical behaviour, even before external symptoms appear. Softening of internal tissues, redistribution of moisture, and microstructural breakdown alter absorption and scattering properties, creating spectral signatures detectable by hyperspectral imaging (Liang et al., 2025).

Similarly, punctual NIR spectroscopy has successfully classified early mechanical damage in kiwifruit with high accuracy using ensemble learning, confirming the detectability of subtle bruise-related spectral changes (Ma et al., 2025). The discriminating power of our PLS-DA model, even when calibrated with a limited number of spectra, indicates that these spectral differences are sufficiently robust to be captured under standard HSI conditions.

Further mechanisms of damage-related spectral variability have been reported in other fruit species, where HSI has successfully detected early damage associated with firmness loss, cell rupture, and water migration (Cen et al., 2012; Zhang et al., 2020). NIR approaches have linked internal quality changes (texture, soluble solids, dry matter) to spectral signatures in ready-to-eat kiwifruit, supporting their use for post-harvest quality monitoring and shelf-life prediction (Li et al., 2024). More recently, field-applicable spatially resolved Vis-NIR spectroscopy has reliably predicted texture in different kiwifruit cultivars, although punctual spectroscopy is affected by limitations related to skin properties and fruit geometry which can be overcome by imaging approaches (Ma et al., 2026).

The consistency between our results and the literature further confirms the reliability of HSI for early, non-destructive detection of bruising in kiwifruit. The findings demonstrate the effectiveness of this methodology in distinguishing healthy from damaged tissue at early stage, providing a rapid and non-destructive approach for quality assessment in the kiwifruit supply chain.

3.4. Damage degree evaluation

To quantitatively assess tissue degradation over time, the percentage of damaged pixels was determined directly from the results of the PCA + Surface Texture + PLS-DA model (Fig. 4). The percentage of damaged pixels for each sample was calculated by setting the number of pixels at T0 (initial time point) to 0, as no damage was induced at that stage. The subsequent damage values were determined by visual inspection of the images and are summarised in Table 2.

The samples were grouped according to the type of damage applied: CC, SW, and DW. The progression of tissue damage over time was observed in the different groups of damaged samples (SW and DW) as

Table 2
Evolution of damage over time for each sample, expressed as the percentage of pixels classified as damaged. Missing values (–) indicate timepoints where the fruit was not analysed.

Batch	Sample name	T0	T1	T2	T3	T4	T5
1	K1_CC	0	0.11	0.20	0.18	0.09	0.08
1	K2_CC	0	0	0	0	0	0
2	K3_CC	0	0	0	0	0	-
2	K4_CC	0	0	0	0	0	-
1	K5_SW	0	2.01	6.23	8.98	10.21	8.78
1	K6_SW	0	0	0	1.15	3.40	-
2	K7_SW	0	0.71	1.56	4.09	4.66	6.04
2	K8_SW	0	0	0	0.24	3.70	-
1	K9_DW	0	1.02	0.96	4.59	4.79	-
1	K10_DW	0	0.25	2.01	3.24	7.20	8.57
2	K11_DW	0	0.61	2.09	3.45	4.40	3.38
2	K12_DW	0	0.02	0.17	0.50	4.08	10.75

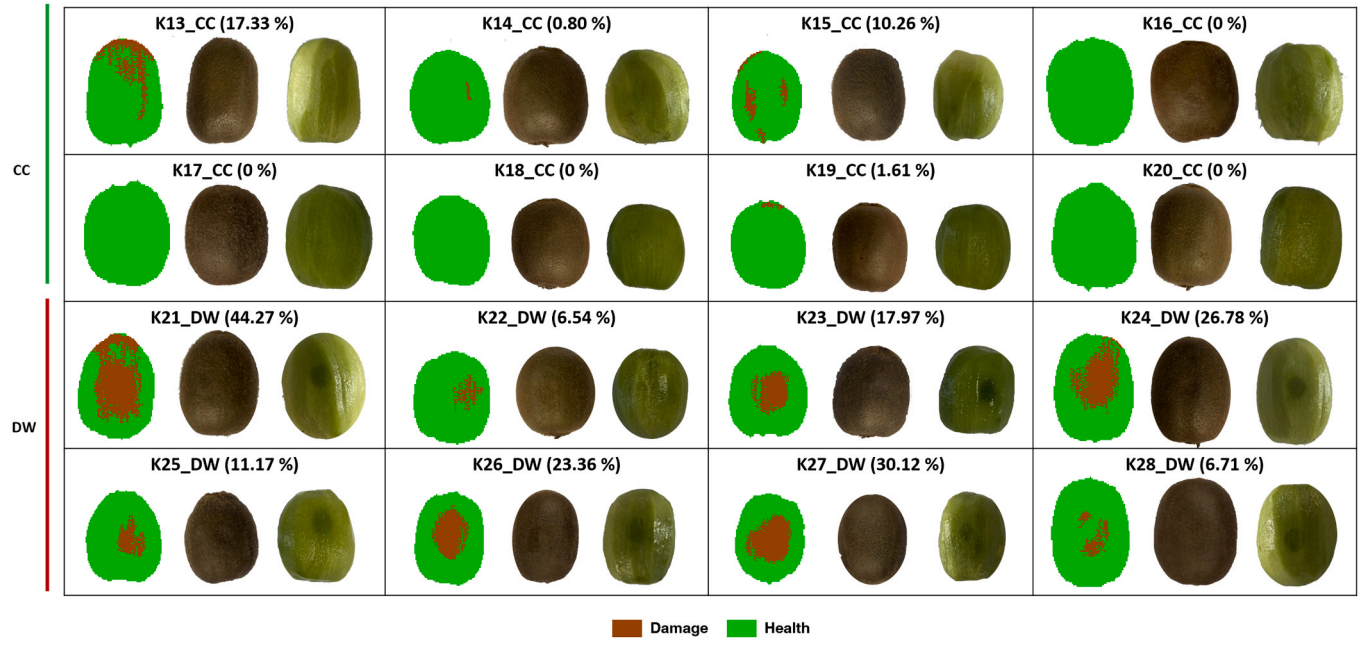

Fig. 5. Comparison of PLS-DA predicted damage with RGB images of whole and peeled fruits from batches 3–5, showing the correspondence between predicted pixels and actual tissue degradation.

reported in Table 2. In the CC group, which served as the control group without mechanically induced stress, the samples (K1_CC, K2_CC, K3_CC, K4_CC) showed little or no increase in damage during the sampling period. The samples remained essentially unchanged; for most of them, no damage at all time points was recorded, confirming the absence of significant degradation. The presence of pixels classified as damaged in sample K1_CC are not indicative of substantial tissue degradation. Indeed, no trend was observed, and the percentage of damaged pixels was low (0.08 – 0.20 %).

The damage progression between the SW and DW groups, subjected to mechanical damage, varied slightly between the samples. Both groups showed an increasing damage trend over time, although the difference between the SW and DW groups was not as pronounced as initially expected. For example, K5_SW showed a steady increase in damage from 2.01 % at T1–8.78 % at T5, indicating progressive tissue degradation like sample K7_SW.

The results suggested that although both the SW and DW groups showed tissue degradation under mechanical stress, the differences between the two groups were minimal in terms of damage progression. This suggests that the severity of the damage may not depend solely on the amount of weight applied, but could also be influenced by other factors, such as the heterogeneity of the sample or the intrinsic properties of the tissue. However, the general trend of increasing damage over time in these groups is consistent with expectations, confirming that mechanical damage leads to progressive tissue degradation.

Importantly, the forces applied (23.4 N and 46.8 N) were significantly lower than in prior studies, mimicking real-world impacts during transport and manual handling. The fact that such light impacts generated detectable degradation over time, validated through spectral and textural evolution, shows that minor mechanical events can trigger measurable internal responses, which can now be monitored non-destructively using NIR-HSI.

These results highlight the complexity of tissue response to mechanical stress and the potential variability of individual samples. The results in Table 2 and Fig. 4 provide a clear visual and quantitative representation of tissue damage over time, supporting the utility of the PCA + Surface Texture + PLS-DA model for monitoring and quantifying changes in tissue degradation. Although no visible bruising was apparent on the fruit surface during storage, internal damage was confirmed upon peeling at the final timepoint, supporting the idea that some bruises remained undetectable by normal visual inspection.

From a practical perspective, although commercial fruit sorters currently employ infrared (NIR)-based systems, typically using illumination at around 900 nm combined with computer vision and artificial intelligence for bruise detection, these methods often have accuracy limitations, especially for minor or internal damage in kiwifruit. Our study builds on these commercial approaches and demonstrates that, by using a broader hyperspectral range, higher spatial resolution, and advanced multivariate analysis, it is possible to achieve earlier and more accurate detection of mechanical damage under realistic impact conditions.

4. Conclusions

This study demonstrates the feasibility and added value of combining Near-Infrared Hyperspectral Imaging (NIR-HSI) with surface textural analysis and multivariate classification for the early, non-destructive detection and temporal monitoring of mechanical damage in kiwifruit, even under low-impact, realistic force conditions.

Integrating surface texture features extracted from PCA score images, which enhanced the spatial resolution of damage detection, enhanced the detection of structural alterations in the fruit. These features captured subtle structural deformations, particularly those not visible to the naked eye or detectable using traditional NIR approaches. This spatial enhancement, combined with spectral data, enabled the detection of incipient internal damage and the monitoring of bruise evolution over several days, providing a realistic simulation of post-harvest storage and handling.

The classification results using PLS-DA confirm the robustness of the combined PCA-surface-texture approach, achieving high accuracy in identifying damaged areas across different stages of progression. The 2025 dataset further validated the model's predictive capability, demonstrating that the methodology can reliably detect early bruising in new samples collected under the same experimental conditions.

Notably, the study reveals that damage progression depends not only on the magnitude of the impact force but also on fruit heterogeneity and tissue response over time. Quantifying damage severity and its temporal evolution provides valuable insights for optimising post-harvest handling strategies that support improved sorting, redistribution, and valorization of affected fruit, thereby limiting avoidable consumer-level waste.

Overall, this research supports the adoption of hyperspectral imaging as a powerful tool for automated, non-destructive quality control in the fruit industry. Implementing such technology in processing lines could enhance the selection process, ensuring that compromised fruit is identified before reaching the market, while also enabling alternative uses for damaged produce. This approach aligns with modern demands for sustainable food production by reducing avoidable consumer-level waste through improved sorting and valorization strategies, while enhancing consumer satisfaction with high-quality, undamaged fruits.

Future work should focus on expanding the dataset with a larger number of samples and integrating this methodology into real-time, inline systems, further exploring its application across different fruit varieties and damage scenarios.

CRediT authorship contribution statement

Silvia Grassi: Writing – review & editing, Visualization, Methodology, Investigation, Data curation, Conceptualization. **Irene Locatelli:** Writing – original draft, Validation, Methodology, Investigation, Data curation. **Giulia Gorla:** Writing – review & editing, Methodology, Investigation, Formal analysis. **Alessandro Grassi:** Investigation, Formal analysis. **José Manuel Amigo:** Writing – review & editing, Visualization, Methodology, Investigation, Data curation, Conceptualization.

Funding

The authors declare that no funds. grants or other support were received during the preparation of the submitted work.

Declaration of Competing Interest

The authors declare that they have no known competing financial interests or personal relationships that could have appeared to influence the work reported in this paper.

Data availability

Data will be made available on request.

References

Adewoyin, O.B., 2023. Pre-harvest and postharvest factors affecting quality and shelf life of harvested produce. New Advances in Postharvest Technology. IntechOpen. https://doi.org/10.5772/intechopen.111649.

Ahmadi, E., 2012. Bruise susceptibilities of kiwifruit as affected by impact and fruit properties. Res. Agric. Eng. 58, 23–29. https://doi.org/10.17221/57/2011-RAE.

Amigo, J.M., 2019. Hyperspectral imaging, 32. Elsevier.

Arbash, E., de Lima Ribeiro, A., Thiele, S., Gnann, N., Rasti, B., Fuchs, M., Ghamisi, P., Gloaguen, R., 2023. Masking hyperspectral imaging data with pretrained models. 13th Workshop on Hyperspectral Imaging and Signal Processing: Evolution in Remote Sensing (WHISPERS). IEEE, pp. 1–5. https://doi.org/10.1109/whispers61460.2023.10431074.

Barrett, D.M., Beaulieu, J.C., Shewfelt, R., 2010. Color, flavor, texture, and nutritional quality of fresh-cut fruits and vegetables: desirable levels, instrumental and sensory measurement, and the effects of processing. Crit. Rev. Food Sci. Nutr. 50, 369–389. https://doi.org/10.1080/10408391003626322.

Bharati, M.H., Liu, J.J., MacGregor, J.F., 2004. Image texture analysis: methods and comparisons. Chemom. Intell. Lab. Syst. 72, 57–71. https://doi.org/10.1016/j.chemolab.2004.02.005.

Bu, Y., Luo, J., Li, J., Chi, Q., Guo, W., 2024a. Detection of hidden bruises on kiwifruit using hyperspectral imaging combined with deep learning. Int. J. Food Sci. Technol. 59, 5975–5984. https://doi.org/10.1111/ijfs.17256.

Bu, Y., Luo, J., Li, J., Yang, S., Chi, Q., Guo, W., 2024b. Non-destructive estimation of the bruising time in kiwifruit based on spectral and textural data fusion by machine learning techniques. J. Food Meas. Charact. 18, 6872–6885. https://doi.org/10.1007/s11694-024-02699-0.

Cen, H., Lu, R., Mendoza, F.A., Ariana, D.P., 2012. Assessing multiple quality attributes of peaches using optical absorption and scattering properties. Trans. ASABE 55, 647–657. https://doi.org/10.13031/2013.41366.

Cheng, J., Guo, W., Du, R., Zhou, Y., 2022. Optical properties of different kiwifruit cultivars (*Actinidia deliciosa* and *Actinidia chinensis*) and their correlation with internal quality. Infrared Phys. Technol. 123, 104113. https://doi.org/10.1016/j.infrared.2022.104113.

Ciccoritti, R., Paliotta, M., Amoriello, T., Carbone, K., 2019. FT-NIR spectroscopy and multivariate classification strategies for the postharvest quality of green-fleshed kiwifruit varieties. Sci. Hortic. 257, 108622. https://doi.org/10.1016/j.scienta.2019.108622.

Delwiche, S.R., Baek, I., Kim, M.S., 2021. Effect of curvature on hyperspectral reflectance images of cereal seed-sized objects. Biosyst. Eng. 202, 55–65. https://doi.org/10.1016/j.biosystemseng.2020.11.004.

Ebrahimi, S., Pourdarbani, R., Sabzi, S., Rohban, M.H., Arribas, J.I., 2023. From harvest to market: Non-destructive bruise detection in kiwifruit using convolutional neural networks and hyperspectral imaging. Horticulturae 9, 936. https://doi.org/10.3390/horticulturae9080936.

Fu, X., Ying, Y., Lu, H., Xu, H., Yu, H., 2007. FT-NIR diffuse reflectance spectroscopy for kiwifruit firmness detection. Sens. Instrum. Food Qual. Saf. 1, 29–35. https://doi.org/10.1007/s11694-007-9004-2.

Gao, M., Guo, W., Huang, X., Du, R., Zhu, X., 2021. Effect of pressing and impacting bruises on optical properties of kiwifruit flesh. Postharvest Biol. Technol. 172, 111385. https://doi.org/10.1016/j.postharvbio.2020.111385.

Gaston, E., Frias, J.M., Cullen, P.J., O'Donnell, C.P., Gowen, A.A., 2010. Prediction of polyphenol oxidase activity using visible near-infrared hyperspectral imaging on mushroom (Agaricus bisporus) caps. J. Agric. Food Chem. 58, 6226–6233. https://doi.org/10.1021/jf100501q.

Gowen, A.A., O'Donnell, C.P., Cullen, P.J., Downey, G., Frias, J.M., 2007. Hyperspectral imaging–an emerging process analytical tool for food quality and safety control. Trends Food Sci. Technol. 18, 590–598. https://doi.org/10.1016/j.tifs.2007.06.001.

Hou, J., He, Z., Liu, D., Zhu, Z., Long, Z., Yue, X., Wang, W., 2023. Mechanical damage characteristics and nondestructive testing techniques of fruits: a review. Food Sci. Technol. 43, e001823. https://doi.org/10.1590/fst.001823.

Koutsoflini, A., Gerasopoulos, D., Vasilakakis, M., 2013. The effects of fruit maturation, delayed storage and ethylene treatment on the incidence of low-temperature breakdown of 'Hayward' kiwifruit. J. Sci. Food Agric. 93 (2), 410–414. https://doi.org/10.17660/ActaHortic.2011.913.73.

Liang, D., Wang, N., Yin, H., Cui, J., Huang, Y., Sun, Y., Hu, Y., 2025. Assessment of the optical response of bruised kiwifruit using hyperspectral imaging and its relationships with water migration. Postharvest Biol. Technol. 225, 113515. https://doi.org/10.1016/j.postharvbio.2025.113515.

Li, H., Zhu, L., Li, N., Liu, Z., Wang, L., Chitrakar, B., Xu, D., Cui, Z., Tang, Y., Hu, L., Mo, H., 2024. NIR spectroscopy for quality assessment and shelf-life prediction of kiwifruit. Postharvest Biol. Technol. 218, 113201. https://doi.org/10.1016/j.postharvbio.2024.113201.

Liu, Y., Yang, Z., Cao, J., Ling, W.K., Liu, Q., 2019. Detection of Invisible Damage of Kiwi Fruit Based on Hyperspectral Technique. International Conference on Brain Inspired Cognitive Systems. Springer International Publishing, Cham, pp. 373–382. https://doi.org/10.1007/978-3-030-39431-8.

Lü, Q., Tang, M.J., Cai, J.R., Zhao, J.W., Vittayapadung, S., 2011. Vis/NIR hyperspectral imaging for detection of hidden bruises on kiwifruits. Czech J. Food Sci. 29, 595–602. https://doi.org/10.17221/69/2010-CJFS.

Ma, T., Xia, Y., Inagaki, T., Tsuchikawa, S., 2021. Non-destructive and fast method of mapping the distribution of the soluble solids content and pH in kiwifruit using object rotation near-infrared hyperspectral imaging approach. Postharvest Biol. Technol. 174, 111440. https://doi.org/10.1016/j.postharvbio.2020.111440.

Ma, T., Inagaki, T., Tsuchikawa, S., Jiang, H., 2026. A field-deployable spectroscopic approach for optimizing kiwifruit harvest timing and postharvest quality management. Postharvest Biol. Technol. 231, 113888. https://doi.org/10.1016/j.postharvbio.2025.113888.

Ma, P., Sun, J., Cong, S., Dai, C., Cai, Z., Yao, K., Zhou, X., Wu, X., Liu, J., 2025. Detection of early damage in kiwifruit based on near-infrared technology. J. Food Process Eng. 48 (5), e70130. https://doi.org/10.1111/jfpe.70130.

Magwaza, L.S., Opara, U.L., Nieuwoudt, H., Cronje, P.J., Saeys, W., Nicolaï, B., 2012. NIR spectroscopy applications for internal and external quality analysis of citrus fruit—a review. Food Bioprocess Technol. 5, 425–444. https://doi.org/10.1007/s11947-011-0697-1.

Mahanti, N.K., Pandiselvam, R., Kothakota, A., Chakraborty, S.K., Kumar, M., Cozzolino, D., 2022. Emerging non-destructive imaging techniques for fruit damage detection: Image processing and analysis. Trends Food Sci. Technol. 120, 418–438. https://doi.org/10.1016/j.tifs.2021.12.021.

Manley, M., McGoverin, C.M., Engelbrecht, P., Geladi, P., 2012. Influence of grain topography on near infrared hyperspectral images. Talanta 89, 223–230. https://doi.org/10.1016/j.talanta.2011.11.086.

Mobaraki, N., Amigo, J.M., 2018. HYPER-Tools. A graphical user-friendly interface for hyperspectral image analysis. Chemom. Intell. Lab. Syst. 172, 174–187. https://doi.org/10.1016/j.chemolab.2017.11.003.

Ozaki, Y., Huck, C., Tsuchikawa, S., Engelsen, S.B., 2020. Near-Infrared Spectroscopy: Theory, Spectral Analysis, Instrumentation, and Applications. Springer Nature. https://doi.org/10.1007/978-981-15-8648-4.

Tanzilli, D., Cocchi, M., Amigo, J.M., D'Alessandro, A., Strani, L., 2024. Does hyperspectral always matter? A critical assessment of near infrared versus hyperspectral near infrared in the study of heterogeneous samples. Curr. Res. Food Sci. 9, 100813. https://doi.org/10.1016/j.crfs.2024.100813.

Zhang, M., Jiang, Y., Li, C., Yang, F., 2020. Fully convolutional networks for blueberry bruising and calyx segmentation using hyperspectral transmittance imaging. Biosyst. Eng. 192, 159–175. https://doi.org/10.1016/j.biosystemseng.2020.01.018.